Abstract ID: 48488

Dose distributions in heterogeneous geometries irradiated by small non-equilibrium megavoltage photon fields

Sudhir Kumar[1], Alan E Nahum[2], Indrin J Chetty[1]

[1]Department of Radiation Oncology, Henry Ford Health System, 2799 W. Grand Boulevard, Detroit, MI, [2]12 Beech House, Ancastle Green, Henley-on-Thames, United Kingdom

1. INTRODUCTION

The loss of charged-particle equilibrium (CPE), together with the 'geometrical' phenomenon of 'source occlusion' (due to the finite size of the effective x-ray source) makes the dosimetry of small, sub-equilibrium megavoltage photon fields problematic, compared to the well-established dosimetry procedures for 'large' fields.[1-3] In this study, the absorbed dose in bone- and lung-equivalent material embedded in water, compared to that in *uniform* water, is investigated from 'large' to very small field sizes for 6 MV and 15 MV photon beams. We have also determined the range of field sizes at which quasi-CPE is lost in bone and lung-equivalent materials. Ultimately the aim is to quantify possible errors in non-Monte Carlo based treatment plans involving heterogeneities such as lung and bone in small fields.

2. METHODS AND MATERIALS

Previously validated Monte-Carlo (MC) models of a Varian 2100C and 2100 iX linear accelerators for 15 MV and 6 MV photon beams respectively have been employed.[4-5]

2.A. Computation of absorbed dose as a function of depth and field size

Cylindrical phantoms (outer radius 15 cm, height 30 cm) consisted of 3 cm water, then 7 cm lung-equivalent material (ρ = 0.21 g cm^{-3}) then 20 cm water (Fig. 1B) ***and*** of 3 cm water, then 2 cm bone-equivalent material (ρ = 1.8 g cm^{-3}), then 25 cm water (Fig. 1A). Additionally, a homogeneous (water) phantom of the same dimensions was modelled.

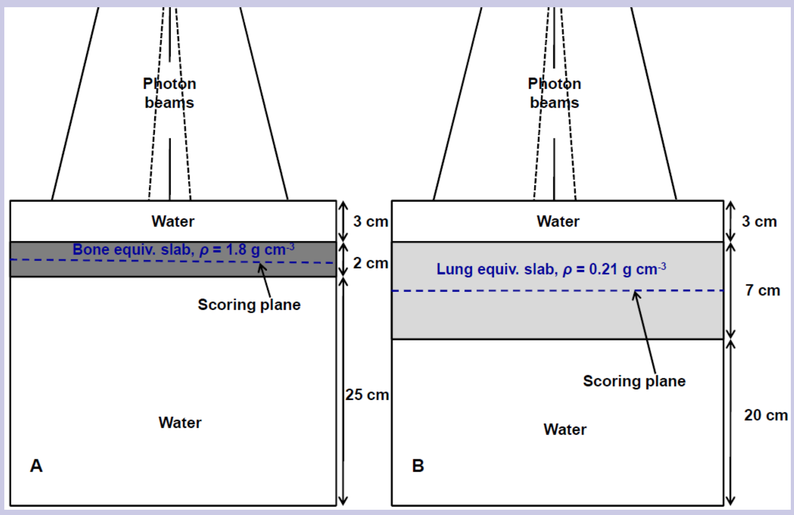

FIG. 1. Schematic diagram illustrating the calculation geometries with bone-equivalent and lung-equivalent material in bone-equivalent and lung-equivalent slab phantoms respectively (A – bone; B – lung).

The absorbed dose, D, in the heterogeneous and homogeneous phantoms at various depths along the beam axis was derived from the EGSnrc Monte-Carlo user-code DOSRZnrc[6] with *ECUT* (electron/positron total energy cut-off) = 512 keV and *PCUT* (photon energy cut-off) = 1 keV, for field sizes, *FS*, of 0.25 × 0.25 to 7 × 7 cm^2 (6 MV) and 0.25 × 0.25 to 16 × 16 cm^2 (15 MV) defined at 100 cm source to phantom surface distance (SSD), using *full linac geometry* phase-space files generated for these field sizes. The scoring volume was a 'point like' cylinder with a circular cross-section of 0.5 mm diameter (to minimize volume-averaging) and a) 0.5 mm height in the build-up region, interface regions and lung- and bone-like media, (b) 2 mm height at other depths, centred on the beam central axis.

2.B. Quantifying the loss of charged particle equilibrium in heterogeneous media

The absorbed-dose to collision-kerma ratio, D/K_{col}, is a measure of the degree of (quasi) CPE. D/K_{col} was calculated in bone and in lung in the heterogeneous phantoms (Fig. 1) and at the same depth in a homogeneous (water) phantom on the central axis in cylindrical phantoms for both beam qualities.

User-code DOSRZnrc[6] does not score K_{col}; we obtained the ratio (K_{col}/K) by computing the 'photon cavity integrals' given below (Eqs. (1) and (2)). The total photon fluence, per MeV per incident photon fluence, down to 1 keV, with the same *ECUT* and *PCUT* as above, was scored in a volume through the centre of either bone or lung at 3.957 cm depth (in bone-equivalent medium) and 6.475 cm depth (in lung-equivalent medium) along the central axis of the heterogeneous cylindrical phantoms (Fig. 1) for the both beams and the full range of field sizes described above, using the user-code FLURZnrc[6]. Kermas K and K_{col} were then calculated over the (energy) fluence spectrum from the following expressions:

$$\left[K(z)\right]_{med} = \int_{PCUT}^{k_{max}} k\left[\Phi_k^{phot}(z)\right]_{med}\left(\frac{\mu_{tr}(k)}{\rho}\right)_{med} dk \qquad (1)$$

and

$$\left[K_{col}(z)\right]_{med} = \int_{PCUT}^{k_{max}} k\left[\Phi_k^{phot}(z)\right]_{med}\left(\frac{\mu_{en}(k)}{\rho}\right)_{med} dk \qquad (2)$$

where k is the photon energy, $\mu_{tr}(k)/\rho$ and $\mu_{en}(k)/\rho$ are the mass energy-transfer and the mass energy-absorption coefficients respectively, and $\left[\Phi_k^{phot}(z)\right]_{med}$ is the photon fluence, differential in energy, as a function of depth z in the medium. From Eqs. (1) and (2) , K_{col}/K = (1- $\overline{g}$) was calculated at the depths specified above in the heterogeneous cylindrical phantoms and then multiplied by K computed by DOSRZnrc (at the same depth and in the same medium), to yield K_{col} as a function of *FS* for each medium.

D/K_{col} could then be obtained as a function of field size using D computed at same depth and in the same medium. In addition to the bone-equivalent and lung-equivalent media, D/K_{col} ratios were derived for homogeneous water at depths of 3.975 cm and 6.475 cm for both beams at the full range of field sizes described above.

2.C. Inhomogeneity dose-perturbation factor as a function of field size

The inhomogeneity dose perturbation factor, *DPF* is defined as the ratio of the dose in the heterogeneous phantom, $D(z)_{hetero}$, at depth, z, to the dose in the homogeneous water phantom, $D(z)_w$, at the same physical depth, z, and for the same beam quality:

$$\left[DPF(z)\right]_w^{hetero} = \frac{D(z)_{hetero}}{D(z)_w} \qquad (3)$$

where 'hetero' and 'w' indicate the heterogeneous (water-bone/lung-water) and homogeneous water phantoms, respectively. The *DPF*s quantify the effect of the inhomogeneity on the dose elative to that in uniform water at the same depth. The *DPF*s were derived from Eq (3) at 3.975 cm depth in bone and 6.475 cm in lung along the beam central axis in both beams.

3. RESULTS

3.A. Absorbed dose as a function of depth and FS

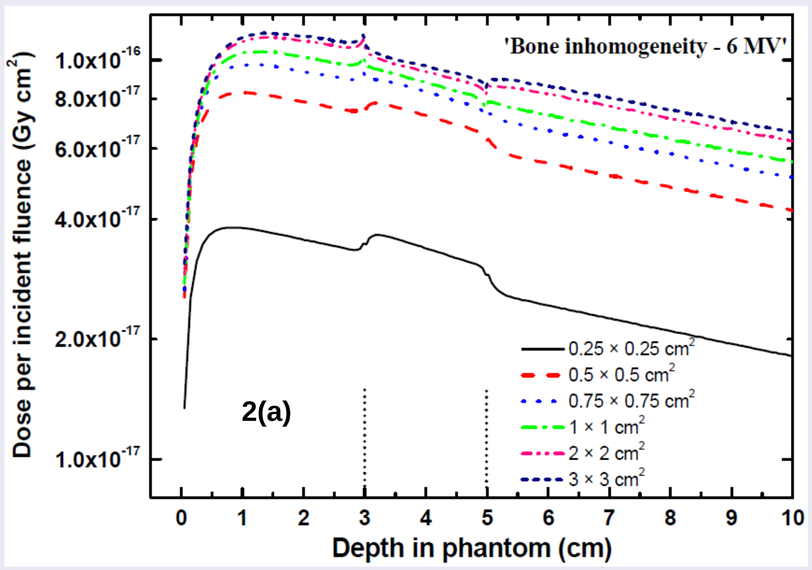

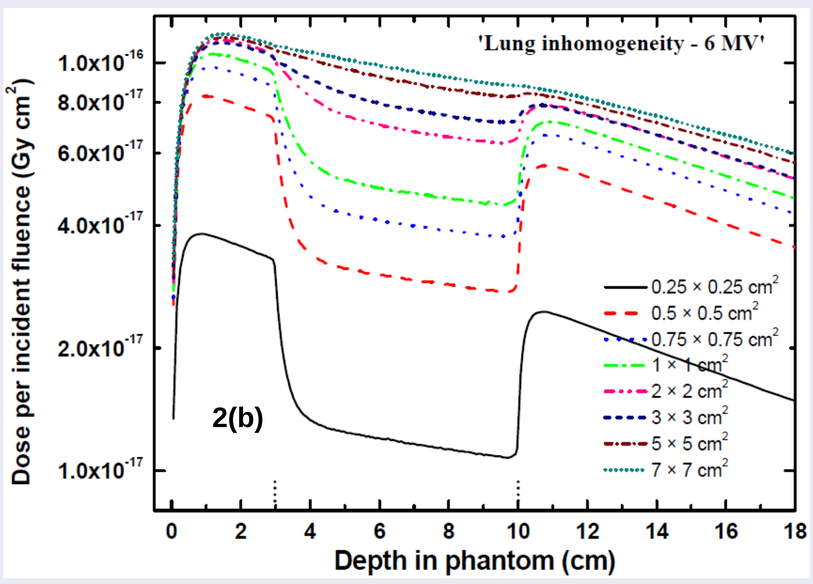

FIGS. 2(a)-(b). Absorbed dose computed in a water-inhomogeneity-water phantom from the surface to the maximum depth (0 - 30 cm) along the central axis of the 6 MV beam, with field sizes ranging from 0.25 × 0.25 to 7 × 7 cm^2 (a – bone; b – lung).

In Fig. 2 (a), dose build-up and dose build-down are seen at the proximal and distal ends of the bone inhomogeneities respectively; in Fig. 2(b), the dose build-down and build-up occur at the proximal and distal end respectively of the lung inhomogeneity. The dose *build-up* (≤ 0.75 × 0.75 cm^2) at the proximal end of the bone inhomogeneity is due partly to backscattering of the secondary electrons from bone which has a higher atomic number than water. The dose *build-down* (≤ 0.75 × 0.75 cm^2) at distal end of the bone inhomogeneity is partly attributable to decreased backscattering of the secondary electrons from the water. In lung these effects are reversed. A similar pattern is observed at 15 MV, though in this case the (lateral) electronic disequilibrium is amplified because of the greater electron range compared to 6 MV.

In the bone inhomogeneity the dose is increased (vs. homogeneous water) for field size < 1 × 1 cm^2 at 6 MV and ≤ 3 × 3 cm^2 at 15 MV; at 0.25 × 0.25 cm^2 field size and 3.975 cm depth dose enhancements of 10.8% at 6 MV and 28.7% at 15 MV were obtained – this can be explained in terms of *reduced* (lateral) electronic disequilibrium in bone compared to the overlying and underlying water regions due to higher mass density of bone. Also in bone, now at the *quasi-equilibrium* field size ≥ 0.75 × 0.75 cm^2 at 6 MV and ≥ 5 × 5 cm^2 at 15 MV the dose is *reduced* (vs. homogeneous water) both at 3.975 cm depth – this is due to the slightly lower value of $\mu_{en}(k)/\rho$ in bone compared to water. In the lung inhomogeneity, dose *reductions* (vs. homogeneous water) of 53% (6 MV) and 67.3% (15 MV) were seen at 6.475 cm depth in the 0.25 cm field, due to *increased electronic disequilibrium* in the lower density lung, compared to in water. However, dose reduction (vs. homogeneous water) in the lung inhomogeneity is negligible for field size > 5 × 5 cm^2 at 6 MV and > 16 × 16 cm^2 at 15 MV, as there is partial CPE.

3.B. D/K_{col} as function of FS

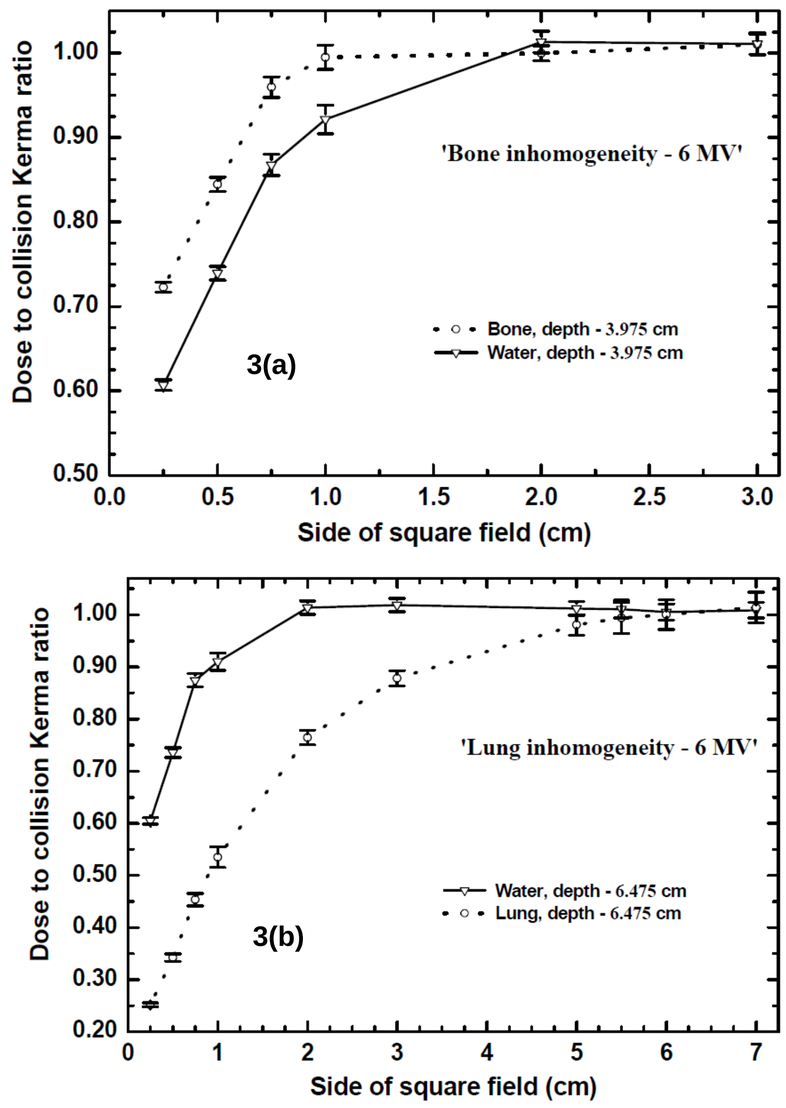

FIGS. 3(a)-(b). 6 MV: MC-derived D/K_{col} ratios vs, FS, at the centre of the heterogeneous media (a – bone; b - lung) in water and in homogeneous water on the central axis at same physical depth.

From Figs 3(a)-(b), it is observed that D/K_{col} decreases rapidly as the field size decreases below about 1 × 1 cm^2 in bone and 5 × 5 cm^2 in lung. These decreases are to the result of the onset of (lateral) electronic *dis*equilibrium as the field width becomes too small to encompass the lateral excursions of the highest energy secondary electrons. The figures demonstrate that CPE is achieved in bone for FS ≥ 1 × 1 cm^2 at 6 MV and ≥ 5 × 5 cm^2 at 15 MV; in lung CPE is achieved at FS > 5 × 5 cm^2 at 6 MV and ≥ 16 × 16 cm^2 at 15 MV.

3.C. MC-derived *DPFs* as function of FS

TABLE I. MC-derived *DPFs* bone-to-water, and lung-to-water, computed using Eq. (3) at depths of 3.975 cm (bone) and 6.475 cm (lung) vs. FS for both beams. The Type A uncertainties are ± 2 standard deviations.

Field Size (cm × cm)	Monte-Carlo-derived dose-perturbation factors, Bone-to-water 6 MV	Bone-to-water 15 MV	Lung-to-water 6 MV	Lung-to-water 15 MV
0.25 × 0.25	1.108 ± 0.003	1.287 ± 0.013	0.470 ± 0.002	0.327 ± 0.002
0.5 × 0.5	1.065 ± 0.005	1.237 ± 0.007	0.519 ± 0.003	0.359 ± 0.003
0.75 × 0.75	1.022 ± 0.006	1.193 ± 0.007	0.587 ± 0.004	0.401 ± 0.002
1 × 1	0.988 ± 0.006	1.159 ± 0.005	0.642 ± 0.005	0.432 ± 0.002
2 × 2	0.945 ± 0.005	1.075 ± 0.003	0.819 ± 0.005	0.537 ± 0.002
3 × 3	0.948 ± 0.007	1.032 ± 0.005	0.886 ± 0.005	0.633 ± 0.003
5 × 5	--------	0.993 ± 0.004	0.999 ± 0.007	-------
10 × 10	--------	0.992 ± 0.004	-------	0.949 ± 0.004
16 × 16	--------	----------	-------	1.016 ± 0.003

Constant dose-perturbation factors are reached for FS ≥ 2 × 2 cm^2 (6 MV) and ≥ 5 × 5 cm^2 (15 MV) in bone and ≥5 × 5 cm^2 and ≥16 × 16 cm^2 in lung at 6 MV and 15 MV respectively; hence at these large field sizes density differences no longer play any role.

4. CONCLUSIONS

The behaviour of the absorbed dose in heterogeneous media irradiated by small *sub-equilibrium* megavoltage photon fields is complex. Once the field is large enough for quasi-CPE to be established in the heterogeneity, the dose is consistent with that predicted by 'large photon cavity' theory. These Monte-Carlo simulations contribute to an improved understanding of the impact of tissue heterogeneity in small, sub-equilibrium photon fields; our results are consistent with those of Scott et al.[7]

REFERENCES

1. Das IJ, et al. *Med. Phys*. 2008; 35**:** 206-215.
2. Aspradakis MM, et al. *IPEM Report no. 103*. York, UK: IPEM; 2010.
3. Palmans H, et al. An IAEA-AAPM International Code of Practice for Reference and Relative Dose Determination. TRS 483: 2017.
4. Scott AJD, et al. *Med. Phys.* 2008*;* 35**:** 4671-4684.
5. Underwood TSA, et al. *Med. Phys. 2013;* 40: 082102.
6. Rogers DWO, et al. NRC user codes for EGSnrc. NRC Technical Report PIRS-702 (rev C), ; 2019.
7. Scott AJD, et al. *Phys*. *Med. Biol*. 2012*;* 57: 4461-4476.

Presented at AAPM Spring Clinical Meeting, 4-7 April 2020, Minneapolis **Corresponding author**: skumar23@hfhs.org **This work was supported by a research grant from Varian Medical Systems, Palo Alto, CA.**